TRAJECTORY DESIGN OF A SPACECRAFT FORMATION FOR SPACE-BASED SOLAR POWER USING SEQUENTIAL CONVEX PROGRAMMING

Ashish Goel[*], Soon-Jo Chung[†], and Sergio Pellegrino[‡]

The concept of collecting solar power in space and transmitting it to the Earth using microwaves has been studied by numerous researchers in the past. The Space Solar Power Initiative (SSPI) at Caltech is a collaborative project to bring about the scientific and technological innovations necessary for enabling a space-based solar power system. The proposed system comprises an array of ultra-light, membrane-like deployable modules with high efficiency photovoltaic (PV) concentrators and microwave transmission antennas embedded in the structure. Each module is 60m $\times$ 60m in size and in the final configuration, hundreds of these modules span a 3km $\times$ 3km array in a geosynchronous orbit. As this formation goes around the Earth, the orientation and position of each module has to be changed so as to optimize the angle made by the photovoltaic surface with respect to the sun and by the antenna surface with respect to the receiving station on Earth. In order to achieve high antenna array efficiency, the modules have to remain in a tight formation with an edge-to-edge distance on the order of a few meters. In addition, the modules also have to avoid collisions and maintain a planar configuration to avoid the possibility of both PV and RF shadowing. In this paper, we present the trajectory design that achieves the dual goal of minimizing the propellant usage and maximizing the power delivered to the ground station, while meeting the various orbital constraints. The optimal control problem is solved using sequential convex programming for a 4 $\times$ 4 formation and the results obtained show that it is possible to maintain the formation for 11 years in a geo-synchronous orbit with relatively small amounts of propellant. This serves as a critical achievement in the path towards realizing the objective of space-based solar power.

INTRODUCTION

The concept of collecting solar power in space and transmitting it to the Earth using microwaves was initially floated in a science fiction magazine by Isaac Asimov[1] and first proposed in a technical paper by P. E. Glaser in 1968.[2] Since then, numerous researchers have proposed architectures and implementation strategies for realizing the dream of space-based solar power.[3–5] As a source of renewable energy, space-based solar power has numerous advantages over terrestrial solar power installations. It is largely independent of the diurnal, seasonal and weather-related variability associated with terrestrial solar power. The near-continuous availability of power also eliminates the need for expensive storage solutions. The ability to use beam forming for directing the microwave power to any location at any point of time makes it a very exciting proposition for resource-starved areas on Earth.

[*]Postdoctoral Researcher, Graduate Aerospace Laboratories, California Institute of Technology, Pasadena, CA 91125.
[†]Associate Professor, Graduate Aerospace Laboratories, California Institute of Technology, Pasadena, CA 91125.
[‡]Professor, Graduate Aerospace Laboratories, California Institute of Technology, Pasadena, CA 91125.

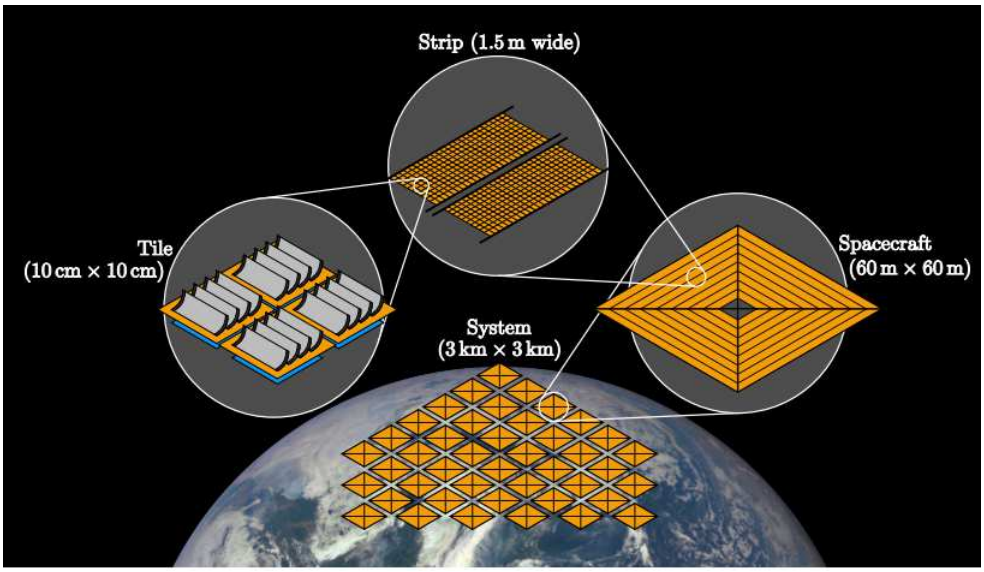

Figure 1. Overview of Space Solar Power System, reproduced from Arya *et al.* (2016).[6] The architecture is modular at multiple levels. The formation comprises a large number of modules. Each module is made up of individual strips that are lined up with identical fundamental units called tiles.

The Space Solar Power Initiative (SSPI) at Caltech is a collaborative project to bring about the scientific and technological innovations necessary for enabling a space-based solar power system. The proposed system comprises an array of ultra-light, membrane-like deployable modules with high efficiency photovoltaic (PV) concentrators and microwave patch antennas embedded in the planar structure. Each module is 60 m $\times$ 60 m in size and in the final proposed configuration, hundreds of these modules span a 3 km $\times$ 3 km array in a geosynchronous orbit. This architecture is depicted in Figure 1, reproduced from Arya *et al.* (2016).[6] Each module is folded and packaged into a 1.5 m $\times$ 1.5 m volume before launch, allowing us to launch multiple modules with a single launch vehicle.[6]

Each module in the formation contains a large number of tiles. The tile is the fundamental unit of this design and comprises two primary layers. The top layer contains a series of parabolic concentrators. Solar radiation incident on these concentrator mirrors gets directed towards a thin strip of photovoltaic cells located on the back side of the concentrators. The DC photocurrent is then converted into microwave radiation at 10 GHz frequency with RF electronic ICs located on the undersides of the top layer. Patch antennas located on the bottom layer of the tile radiate the RF power towards an array of rectifying antennas (rectennas) on Earth. Precision timing control at each of the patch antennas allows them to be operated in the form of a phased array to carry out beam-forming and beam-steering, thereby directing the power towards any desired location on Earth.

As the formation goes around the Earth, the orientation and position of each module has to be changed so as to optimize the angle made by the photovoltaic surface with respect to the sun and by the antenna surface with respect to the receiving station on Earth. Our goal is to carry out these attitude and orbital maneuvers to maximize power transmission while minimizing the propellant mass added to the system. In addition, to achieve high efficiencies in the operation of the phased antenna array, the 60 m $\times$ 60 m modules have to remain in a tight formation, with an edge-to-edge

distance on the order of a few meters. While maintaining this tight formation, the modules also have to avoid collisions and avoid shadowing the neighboring modules in the formation.

A preliminary attempt at designing the optimal trajectories using classical ideas of periodic relative orbits and the Hill Clohessy Wiltshire (HCW) equations was demonstrated by Goel $et\ al.$ in 2017.[7] In this paper, we provide a more rigorous approach by formulating the trajectory design of this formation as an optimization problem and present the results obtained by solving this problem using sequential convex programming. In the following section, we discuss the motivation behind the problem formulation and describe the geometry and setup of the problem. In the next section, we describe how we convexify the various constraints to solve the problem using sequential convex programming. We then describe our results and conclude with a discussion of the results and directions for future research.

As discussed in Goel $et\ al.$ (2010),[7] having a dual-sided module that can transmit RF power from both the top and bottom surfaces or equivalently, a module that can collect solar power from both surfaces can offer a 65% improvement in the orbit-averaged power transmitted to the receiving station on Earth. The dual-sided approach allows the module to operate at a more optimum angle over different orbital positions. Therefore, in this paper, we exclusively present results for these dual-sided modules. The mission duration is assumed to be 11 years and the dry mass of a single spacecraft is estimated to be 370 kg.

PROBLEM FORMULATION

There are numerous challenges associated with trajectory design for SSPI. First, when the modules are ejected from the launch vehicle, we have the problem of creating the formation out of the initial swarm of randomly distributed satellites in space. When the formation is complete, we have the challenge of maintaining the formation using accurate relative position sensors, actuators, and appropriate control framework. Clearly, the satellites that are close to the center of the formation will require less propellant for orbital maneuvering than satellites that are near the extremes of the formation. Therefore, the formation will have to undergo reorganization so that on average, over the course of the proposed lifetime, each module consumes roughly the same amount of propellant. In this paper, we focus our attention on the design of the optimum trajectories for the modules, once the close formation has been achieved. But the same optimal control formulation and solution approach could be used in the future for establishing the initial configuration and for reconfiguration (reorganization maneuvers).

We describe the formation in terms of chief and deputy spacecraft. The chief is a virtual reference whose motion is described in the Earth-Centered Inertial (ECI) reference frame. The chief is in a geosynchronous orbit around the Earth. The real spacecraft (modules) that are actually in the formation are designated as deputies and their motion is described in a local vertical local horizontal (LVLH) frame centered at the chief, as shown in Figure 2. θ is the orbital angle that represents the position of the chief in the geosynchronous orbit. β is the angle made by the planar deputy with the sun and ϕ is the angle made by the deputy with the receiving station on Earth. These three angles are geometrically related as

$$\theta = \beta + \phi \tag{1}$$

The power transmitted (P) by one such deputy to the receiving station depends heavily on the angles θ, β, and ϕ. The orientation that is optimal for collecting the highest amount of solar power

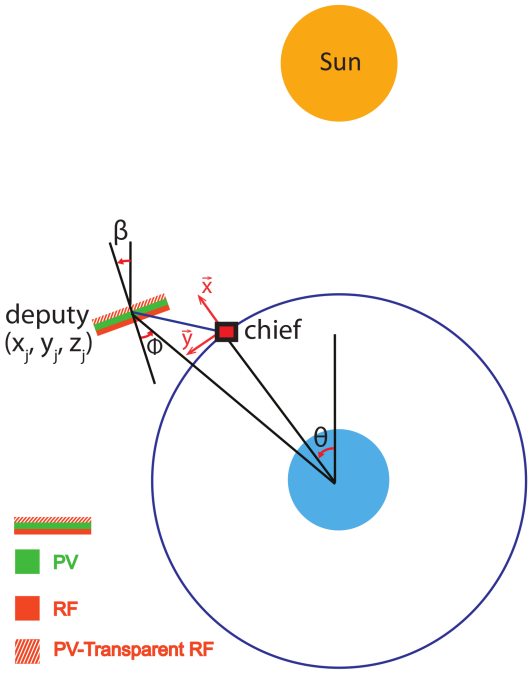

Figure 2. An illustration of chief and deputy spacecraft showing the LVLH frame and the relevant angles θ, β and ϕ.

may not be the most efficient for transmitting the RF power. This dependence can be described as

$$P(\theta, \beta) = P_S \, \eta_{\mathrm{PV}} \, \eta_{\mathrm{DC-RF}} \, \cos(\gamma) \, S(\beta) \, R(\phi) \, \cos(\phi) \tag{2}$$

P_S represents the incident solar flux and is equal to 1361 W/m^2. The second term η_{PV} is the optical power-to-electrical power conversion efficiency of the photovoltaic system and is assumed to be 25%, taking into account the solar cell efficiency and optical efficiency of the concentrators. The term $\eta_{\mathrm{DC-RF}}$ represents the DC-to-RF power conversion efficiency and is assumed to be 33%. The angle γ is the tilt of Earth's equatorial plane with respect to the ecliptic plane and is equal to 23.5°. The P_S, η_{PV}, $\eta_{\mathrm{DC-RF}}$, and $\cos(\gamma)$ terms can all be treated as constants. The next term $S(\beta)$ represents the dependence of photovoltaic efficiency on the angle β and is plotted in Figure 3(a). This profile is obtained using ray tracing simulations of the proposed photovoltaic tile structure. Note that this is a purely geometric effect and should not be confused with the η_{PV} term. The term $R(\phi)$ represents the dependence of the efficiency of a single antenna in the array on the RF angle ϕ. This dependence is obtained using electromagnetic simulations of the antenna and is shown in Figure 3(b). And finally, $\cos(\phi)$ represents the variation of the array factor with ϕ. These factors combine to give a value of $P(\theta, \beta)$ in units of Watts per m^2 of satellite area. Using Equation (1), Equation (2) can be rewritten as

$$P(\theta, \beta) = P_S \, \eta_{\mathrm{PV}} \, \eta_{\mathrm{DC-RF}} \, \cos(\gamma) \, S(\beta) \, R(\theta - \beta) \, \cos(\theta - \beta) \tag{3}$$

Based on this dependence, if we treat θ as a known variable from the chief's orbital motion, we can arrive at the optimum orientation profile for the deputy spacecraft for maximizing power.

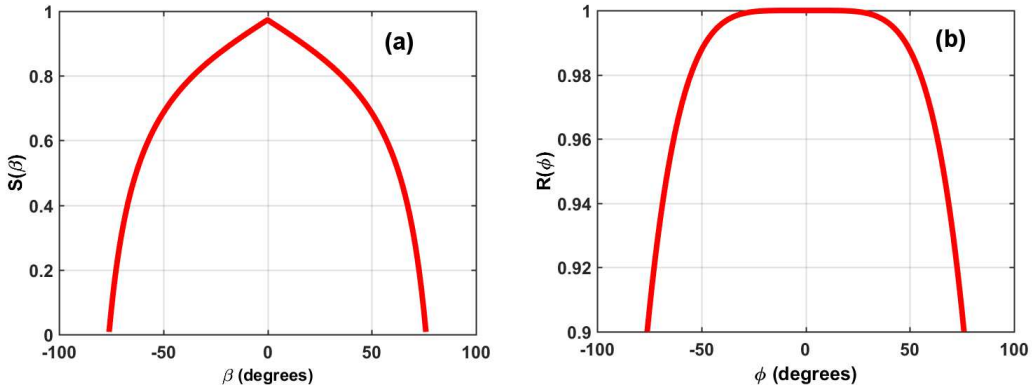

Figure 3. (a) Variation of photovoltaic efficiency with angle β (b) Variation of efficiency of a single antenna in an array with angle ϕ.

However, when considering the entire formation, if each deputy spacecraft only carries out an attitude maneuver, then the satellites would end up shadowing each other, as illustrated in Figure 4. Therefore, the attitude maneuvers that optimize power have to be accompanied by orbital maneuvers which could lead to large propellant mass requirements. This motivates the formulation of the trajectory design as an optimal control problem with the goal of obtaining the right balance between maximizing power and minimizing the mass of the propellant needed to maintain the formation and to carry out the orbital maneuvers accompanying the attitude maneuvers.

If the chief is located at a distance of r from the center of the Earth, then under the action of a control input vector $\boldsymbol{U} = [U_x, U_y, U_z]^T$, the motion of the chief is governed by the following set of equations

$$\ddot{r} - r\dot{\theta}^2 = -\frac{\mu r}{r^3} + a_{SRP}\cos(\theta - \beta) + U_x \tag{4}$$

$$2\dot{r}\dot{\theta} + r\ddot{\theta} = a_{SRP}\sin(\theta - \beta) + U_y \tag{5}$$

where μ is the gravitational parameter. We do not include the z equation for the chief since we restrict its motion to the equatorial plane. Note that we include the acceleration due to solar radiation pressure a_{SRP} since it is the most dominant perturbation force in a geosynchronous orbit given the large area to mass ratio of the spacecraft. The solar radiation pressure has the tendency to ellipticize the chief's orbit and this effect is discussed in more detail by Goel *et al.* (2017),[7] Atchison (2011)[8] and Hamilton & Krivov (1996).[9] While the complete problem formulation would also optimize over the trajectory of the chief spacecraft, in this analysis, we assume that the chief's orbit is known and only optimize the trajectories of the deputy spacecraft. For the sake of simplicity, we assume that the chief is in a geostationary orbit. This makes θ a known quantity in our problem formulation.

We define the relative position vector of the j^{th} deputy spacecraft with respect to the chief (in the LVLH frame) as $\boldsymbol{r}_j = [x_j, y_j, z_j]^T$, the state vector as $\boldsymbol{s}_j = [x_j, y_j, z_j, \dot{x_j}, \dot{y_j}, \dot{z_j}]^T$ and its control input (thrust per unit mass) vector as $\boldsymbol{u}_j = [u_{x_j}, u_{y_j}, u_{z_j}]^T$. In order to avoid the shadowing and obstruction of neighboring spacecraft, we enforce a planarity constraint on the formation. In other words, we stipulate that all the modules have the same orientation for a given orbital angle θ. Although this is only a sufficient and not a necessary condition to avoid shadowing, it allows us

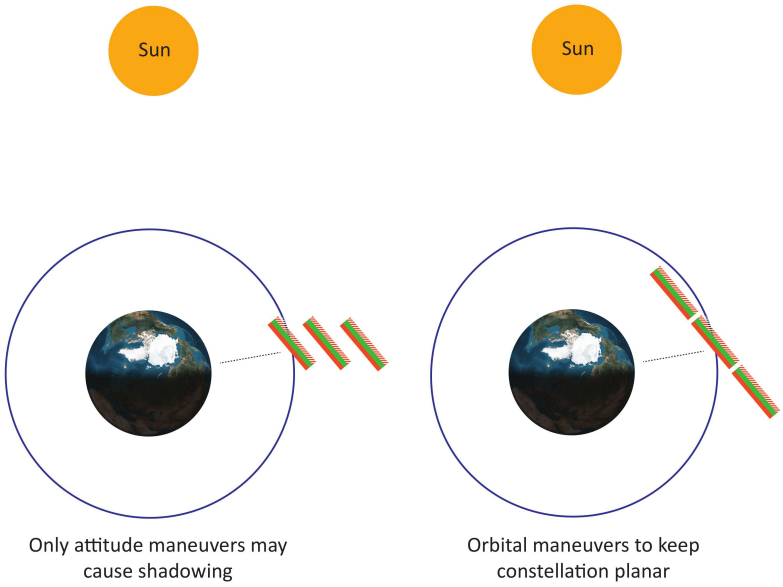

Figure 4. (a) Variation of photovoltaic efficiency with angle β (b) Variation of efficiency of a single antenna in an array with angle ϕ.

to continue using Equation (3) to estimate the power transferred. Otherwise, a full electromagnetic simulation and ray-tracing analysis would have to be carried out to estimate the power transferred for each spacecraft configuration. Since this constraint forces all deputies to have the same orientation, it also ensures that they all experience the same amount of solar radiation pressure at any given point of time. Therefore, the solar radiation pressure term drops out of the dynamics equation for the deputy spacecraft and only appears in the dynamics equations for the chief. In addition, this planarity constraint couples the attitude dynamics of the spacecraft with its orbital motion. This coupling effect is duly accounted for in the formulation of the optimal control problem.

Since gaps in the formation are detrimental to the performance of the phased array, we also enforce an array maintenance constraint whereby the neighboring spacecraft are not allowed to drift too far away from each other. In the future, a detailed electromagnetic model can be incorporated within the optimal control framework to account for this effect but in the current analysis, we simply impose a maximum distance constraint between all neighboring spacecraft. A tree structure is assigned to the formation so that each spacecraft has a unique ID in the formation and has a pre-assigned set of neighbors $\mathcal{N}$.

In addition, we enforce a collision avoidance constraint, boundary conditions and some upper and lower bounds on the values of β, control inputs and speeds of the deputy spacecraft. We also enforce a periodicity constraint so that the performance of the system does not change from day to day. This also allows us to restrict the problem duration to one period of the chief's orbit. And finally, since there are limitations on how quickly such a large spacecraft can change its attitude, we stipulate that two consecutive values of β must not vary by more than $\Delta\beta_{max}$. From Goel *et al.* (2017),[7] we know that carrying out maneuvers at rates on the order of a few deg/s imposes a very small requirement in terms of the propellant needed to carry out the attitude maneuvers using reaction control thrusters. The time step used to discretize the problem is 10 minutes. We hence set the value of $\Delta\beta_{max}$ as 20°.

The optimal control problem for a formation of N satellites can now be formally stated as

Variables: $\boldsymbol{s}_j(k), \boldsymbol{u}_j(k), \beta(k)$ for $j = 1, 2, ..., N; k = 1, 2, ..., T$

Minimize

$$\sum_{j=1}^{N}\sum_{k=1}^{T} \|\boldsymbol{u}_j(k)\|_1 - \lambda \left(\frac{1}{T} \sum_{k=1}^{T} P(\theta(k), \beta(k)) \right)$$

Subject to:

Dynamics

$$\ddot{x}_j(k) - 2\dot{y}_j(k)\dot{\theta}(k) - y_j(k)\ddot{\theta}(k) - x_j(k)\dot{\theta}(k)^2 = -\frac{\mu x_j(k)}{r_j(k)^3} - \mu r(k)(\frac{1}{r_j(k)^3} - \frac{1}{r(k)^3}) + u_{x_j}(k)$$

$$\ddot{y}_j(k) - 2\dot{x}_j(k)\dot{\theta}(k) - x_j(k)\ddot{\theta}(k) - y_j(k)\dot{\theta}(k)^2 = -\frac{\mu y_j(k)}{r_j(k)^3} + u_{y_j}(k)$$

$$\ddot{z}_j(k) = -\frac{\mu z_j(k)}{r_j(k)^3} + u_{z_j}(k)$$

$j = 1, 2, ..., N; k = 1, 2, ..., T$

Boundary Conditions

$\boldsymbol{r}_j(0) = \boldsymbol{r}_{j_0}$

$\boldsymbol{s}_j(T) = \boldsymbol{s}_j(0)$

$\beta(T) = \beta(0)$

$j = 1, 2, ..., N$

Collision Avoidance

$R_{\text{col}} \leq \|\boldsymbol{r}_i(k) - \boldsymbol{r}_j(k)\|$

$i > j; j = 1, 2, ..., N; k = 1, 2, ..., T$

Array Maintenance

$\|\boldsymbol{r}_i(k) - \boldsymbol{r}_j(k)\|_2 \leq D$

$i \in \mathcal{N}_j; j = 1, 2, ..., N; k = 1, 2, ..., T$

Planarity

$x_j(k)\cos(\theta(k) - \beta(k)) = y_j(k)\sin(\theta(k) - \beta(k))$

$j = 1, 2, ..., N; k = 1, 2, ..., T$

Bounds

$\|\dot{\boldsymbol{r}}_j(k)\|_2 \leq V_{max} \quad j = 1, 2, ..., N; k = 1, 2, ..., T$

$|\beta(k)| \leq \beta_{max} \quad k = 1, 2, ..., T$

$\|\boldsymbol{u}_j(k)\|_1 \leq U_{max} \quad j = 1, 2, ..., N; k = 1, 2, ..., T$

$|\beta(k) - \beta(k-1)| \leq \Delta\beta_{max} \quad k = 2, ..., T$

Definitions

- λ chooses the relative weightage between minimizing propellant consumption and maximizing power transfer. Note that we use the $\mathcal{L}_1$ norm in the cost function since we assume that the satellite has individual thrusters in each direction[10]
- r_j is the distance of the jth deputy from the center of the Earth
- $\boldsymbol{r}_{j_0}$ is the initial position of the jth deputy
- D is the maximum separation between two neighboring modules in the formation. This parameter has been set at 115 m
- V_{max}, U_{max} and β_{max} set the maximum absolute values of speed, thrust and β respectively
- R_{col} is the closest allowable distance between any two spacecraft in the formation. It is equal to the size of each spacecraft, $i.e.$ 60 m

SEQUENTIAL CONVEX PROGRAMMING

The $(-P(\theta, \beta))$ term in the cost function, the dynamics equations, the collision avoidance constraint, and the planarity constraint are all non-convex. Further, the combination of the collision avoidance constraint and the array maintenance constraint severely restrict the feasible solution space, making it tough to find the optimum solution. In this paper, we use the sequential convex programming (SCP) algorithm for solving the optimization problem. The basic idea behind SCP is to solve the non-convex problem by making successive convex approximations of the original problem based on the current best estimate of the solution. To illustrate this, let us consider the following non-convex optimization problem

Minimize $f_0(x)$

Subject to: $g_i(x) \leq 0$ for i = 1, 2, ..., m

$h_j(x) = 0$ for j = 1, 2, ... , n

For any intermediate solution $x^{(k)}$, we establish a convex trust region $\tau^{(k)}$ around $x^{(k)}$. We find convex approximations $\hat{f}_0$ of f_0, $\hat{g}_i$ of g_i, and affine approximations $\hat{h}_j$ of h_j over $\tau^{(k)}$ for all i, j. The following convex problem is now solved at each iteration until two successive iterations yield solutions that differ by less than a specified tolerance.

Minimize $\hat{f}_0(x)$

Subject to: $\hat{g}_i(x) \leq 0$ for i = 1, 2, ..., m

$\hat{h}_j(x) = 0$ for j = 1, 2, ... , n

$\|x - x^{(k)}\|_2 \leq \tau^{(k)}$

The advantage of SCP lies in the fact that during each of the iterations, we solve a convex problem whose solution can be found very quickly and accurately. This gives us the ability to scale up the algorithm for large formations, as in the case of the SSPI project. Further, the low computational cost of the implementation allows us to port this algorithm on flight hardware for real-time operations in resource-constrained systems. SCP has been successfully used for robotic motion planning[11,12] and for the guidance and control of swarms of spacecraft in the presence of drag and

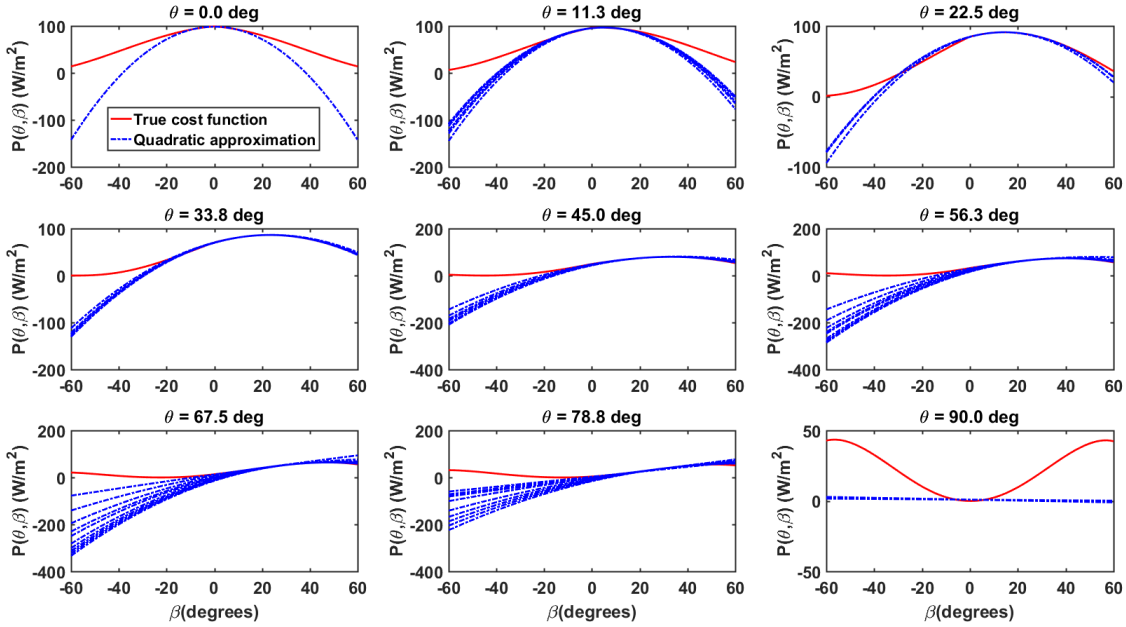

Figure 5. Visualization of the convexification of the cost function over different iterations of SCP. Each dotted curve represents a different approximation based on the value of β from the previous iteration. Different approximations are obtained for different values of θ. We only show the approximation for θ up to 90° since the behaviour of the system is symmetric over the four quadrants during one orbit.

J2 perturbations.[13,14] While SCP does not guarantee finding the global optimum for all types of non-convex optimization problems, it can yield local optimal solutions. For example, Morgan *et al.* (2016)[15] show that the SCP formulation for multi-spacecraft optimal trajectories, with a convexified collision avoidance condition, can be proven to converge to the local optimal point (Karush-Kuhn-Tucker point) of the original non-convex problem.

We now discuss how we go about convexifying each of the four non-convex components in our optimization problem.

Cost Function

The $(-P(\theta,\beta))$ term in the cost function is non-convex and going back to its definition in Equation (3), we know that the non-convex behavior is largely due to the $R(\theta-\beta)$ and $\cos(\theta-\beta)$ terms. In order to convexify this, we restrict the solution space to a small range of angles ($\pm 10°$) around the solution from the previous iteration. Over this range of angles, we use a quadratic approximation of the cost function which is shown using dotted lines for various values of θ in Figure 5. Note that convexifying $(-P(\theta,\beta))$ is equivalent to finding a concave approximation for $P(\theta,\beta)$. In this figure, the quadratic approximation has been plotted for several iterations and it shows how the approximation evolves as the value of β from the previous iteration changes. This scheme results in a changing cost function for every iteration.

Dynamics Equations

Since convex programming requires all equality constraints to be affine, the dynamics equations are linearized about the trajectory from the previous iteration ($\overline{\boldsymbol{s}}_j$). The linearization yields an equation of the following form

$$\dot{\boldsymbol{s}}_j = A(\overline{\boldsymbol{s}}_j)\boldsymbol{s}_j + B(\overline{\boldsymbol{s}}_j)\boldsymbol{u}_j + C(\overline{\boldsymbol{s}}_j) \tag{6}$$

The matrices A, B, and C are obtained by taking the Jacobian of the dynamics equations. By using a zero-order-hold approach to discretize the problem, the linearized form of the dynamics equations can now be written as

$$\boldsymbol{s}_j(k+1) = A_j(k)\boldsymbol{s}_j(k) + B_j(k)\boldsymbol{u}_j + C_j(k) \tag{7}$$

The equations for A_j, B_j, and C_j can be found in Morgan $et\ al.$ (2014)[13] and have been reproduced here in Appendix A. An important point to note here is that the nominal trajectory $\overline{\boldsymbol{s}}_j$ used for linearization is not the solution directly obtained from the previous iteration. Having obtained an optimum thrust vector $\boldsymbol{u}_j$ from the previous iteration, the true non-linear dynamics equations are used to propagate the trajectory with a fourth-order Runge-Kutta method.[16] We thus obtain $\overline{\boldsymbol{s}}_j$, which represents the true trajectory of the spacecraft for the $\boldsymbol{u}_j$ obtained by solving the convex optimization problem. This step can be thought of as the corrector step in a predictor-corrector method and prevents error build-up when large number of iterations are needed to arrive at the final solution. It also ensures that in the last iteration of SCP, when the solution changes by a very small value, the convexified optimization problem is a very good approximation of the original problem.

Collision Avoidance The collision avoidance constraint is concave since it represents a spherical exclusion zone around each spacecraft. The best convex approximation to a concave constraint is affine and hence we replace the spherical boundary with a plane tangent to the sphere and normal to the line joining the two spacecraft. A convex version of collision avoidance is hence implemented by forcing the spacecraft to stay on either sides of this hyperplane boundary. More details about the convexification of the collision avoidance constraint can be found in Morgan $et\ al.$ (2014).[13] Mathematically, the convexified version of the constraint equation for deputies i and j can be written as

$$(\overline{\boldsymbol{r}}_j[k] - \overline{\boldsymbol{r}}_i[k])^T(\boldsymbol{r}_j[k] - \boldsymbol{r}_i[k]) \geq R_{\text{col}}\|\overline{\boldsymbol{r}}_j[k] - \overline{\boldsymbol{r}}_i[k]\|_2 \tag{8}$$

where $\overline{\boldsymbol{r}}_j[k]$ represents the position of the jth deputy at time k, obtained from the previous iteration. The collision avoidance constraint does present a challenge in terms of scalability since one such constraint equation has to be written down for every pair of satellites in the formation. The number of such equations scales with the number of satellites as N^2. The decentralization approach discussed in Morgan $et\ al.$ (2014)[13] cannot be used here since all deputies share the common variable $\boldsymbol{\beta}$.

Planarity Constraint The planarity constraint is also an equality constraint and therefore demands an affine approximation. Reproducing the planarity constraint from the problem formulation, we have

$$x_j \cos(\theta - \beta) = y_j \sin(\theta - \beta) \tag{9}$$

We now define $\tilde{x_j} = x_j - \overline{x}_j$, $\tilde{y_j} = y_j - \overline{y}_j$ and $\tilde{\beta} = \beta - \overline{\beta}$. Equation (9) can now be written as

$$(\overline{x}_j + \tilde{x_j})\cos(\theta - \overline{\beta} - \tilde{\beta}) = (\overline{y}_j + \tilde{y_j})\sin(\theta - \overline{\beta} - \tilde{\beta})$$

If we restrict $\tilde{x_j}$, $\tilde{y_j}$ and $\tilde{\beta}$ to small values, then $\sin(\tilde{\beta})$ can be approximated as $\tilde{\beta}$ and $\cos(\tilde{\beta})$ can be approximated as 1. Ignoring the second order terms, we now have

$$(\overline{x}_j + \tilde{x_j})\cos(\theta - \overline{\beta}) + \overline{x}_j\tilde{\beta}\sin(\theta - \overline{\beta}) = (\overline{y}_j + \tilde{y_j})\sin(\theta - \overline{\beta}) - \overline{y}_j\tilde{\beta}\cos(\theta - \overline{\beta})$$

From the definitions of $\tilde{x_j}$ and $\tilde{x_j}$, we get

$$x_j\cos(\theta - \overline{\beta}) + \overline{x}_j\tilde{\beta}\sin(\theta - \overline{\beta}) = y_j\sin(\theta - \overline{\beta}) - \overline{y}_j\tilde{\beta}\cos(\theta - \overline{\beta})$$

which is linear in x_j, y_j, and β.

Trust Region Update

A critical aspect of sequential convex programming is the introduction of a trust region in the optimization framework. This trust region signifies the region over which we 'trust' our convex approximation. A very large trust region could lead to large convexification errors and inaccurate results while a very small trust region makes the algorithm very slow. There are different approaches used for updating the size of the trust region after each iteration. If the problem is well behaved, fast convergence can be ensured by steadily shrinking the trust region by a constant factor. Since the computation time is not of primary concern for this analysis, we keep the size of the trust region constant.

Due to the restriction of the trust region, in the first few iterations, the algorithm explores the feasible space close to the starting guess used to initiate the algorithm. Therefore, it is critical to choose a feasible starting guess which reduces the likelihood of getting stuck in local minima. For this analysis, we use the results obtained from the linearized equations presented by Goel $et\ al.$ (2017)[7] as the initial values of the optimization variables.

To summarize, the convex version of the optimization problem which is solved during an iteration of the SCP algorithm is shown below. We use CVX[17] with the MOSEK[18] solver for solving the convex problem in each iteration.

Variables: $\boldsymbol{s}_j(k), \boldsymbol{u}_j(k), \beta(k)$ for $j = 1, 2, ..., N$; $k = 1, 2, ..., T$

Minimize

$$\sum_{j=1}^{N}\sum_{k=1}^{T}\|\boldsymbol{u}_j(k)\|_1 - \lambda\left(\frac{1}{T}\sum_{k=1}^{T}\hat{P}(\theta(k), \beta(k))\right)$$

Subject to:

Dynamics

$\boldsymbol{s}_j(k+1) = A_j(k)\boldsymbol{s}_j(k) + B_j(k)\boldsymbol{u}_j + C_j(k)$

$j = 1, 2, ..., N$; $k = 1, 2, ..., T$

Boundary Conditions

$\boldsymbol{r}_j(0) = \boldsymbol{r}_{j_0}$

$\boldsymbol{s}_j(T) = \boldsymbol{s}_j(0)$

$\beta(T) = \beta(0)$

$j = 1, 2, ..., N$

Collision Avoidance

$(\overline{\boldsymbol{r}}_j[k] - \overline{\boldsymbol{r}}_i[k])^T(\boldsymbol{r}_j[k] - \boldsymbol{r}_i[k]) \geq R_{\text{col}}\|\overline{\boldsymbol{r}}_j[k] - \overline{\boldsymbol{r}}_i[k]\|_2$

$i > j; j = 1, 2, ..., N; k = 1, 2, ..., T$

Array Maintenance

$\|\boldsymbol{r}_i(k) - \boldsymbol{r}_j(k)\|_2 \leq D$

$i \in \mathcal{N}(j); j = 1, 2, ..., N; k = 1, 2, ..., T$

Planarity

$x_j \cos(\theta - \overline{\beta}) + \overline{x}_j\tilde{\beta}\sin(\theta - \overline{\beta}) = y_j \sin(\theta - \overline{\beta}) - \overline{y}_j\tilde{\beta}\cos(\theta - \overline{\beta})$

$j = 1, 2, ..., N; k = 1, 2, ..., T$

Bounds

$\|\dot{\boldsymbol{r}}_j(k)\|_2 \leq V_{max} \quad j = 1, 2, ..., N; k = 1, 2, ..., T$

$|\beta(k)| \leq \beta_{max} \quad k = 1, 2, ..., T$

$\|\boldsymbol{u}_j(k)\|_1 \leq U_{max} \quad j = 1, 2, ..., N; k = 1, 2, ..., T$

$|\beta(k) - \beta(k-1)| \leq \Delta\beta_{max} \quad k = 2, ..., T$

Trust Region

$\|\boldsymbol{r}_j - \overline{\boldsymbol{r}}_j\|_2 \leq \tau_r$

$|\beta - \overline{\beta}| \leq \tau_\beta$

Definitions

- $\hat{P}(\theta, \beta)$ is the quadratic approximation of $P(\theta, \beta)$
- τ_r and τ_β are sizes of the trust regions for position and β respectively

RESULTS

In this section, we present the results obtained for a 4 $\times$ 4 formation using the SCP framework described in the previous section. The sixteen satellites start at the nodes of regular 4 $\times$ 4 grid centered at the origin in the y-z plane. The centers of adjacent satellites are initially 100 m apart. First we present the Pareto optimal front (Figure 6) for this formation, which is obtained by solving the problem for different values of λ. The first data point corresponds to the baseline case of $\lambda = 0$ where the attitude and orbital motions are decoupled and the last data point corresponds to the largest value of $\lambda = 1000$ with highest weightage for maximizing power.

As anticipated, generating higher values of orbit-averaged power requires more aggressive attitude maneuvers and consumes more propellant. However, it is important to note that the power generated saturates at a value of around 75 W/m^2. Therefore, we can deliver the maximum possible

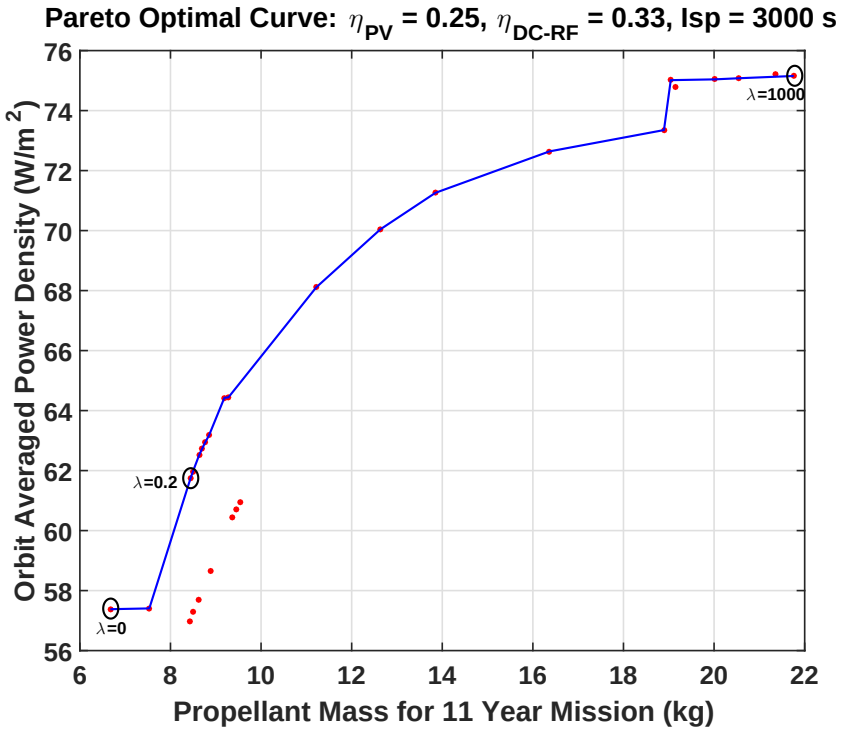

Figure 6. Pareto optimal curve showing the trade-off between power and propellant mass for a satellite in a 4 $\times$ 4 formation. A few data points are marked with the corresponding value of λ.

power from the modules with only 19 kg of propellant for a period of 11 years. In arriving at the estimate of propellant mass from the norm of the $\boldsymbol{u}$ vector, we assume that the orbital maneuvers will be carried out using electric thrusters with an Isp of 3000 s. While current electric propulsion units can reach Isp values on the order of a few thousand seconds, miniaturized versions of such thrusters with Isp of 3000 s are under development[19–22] and could become available when the SSPI modules are ready to be placed in their orbit.

Since SCP does not guarantee finding the global optimum, not all points shown on the graph fall on the Pareto front. A higher density of points has to be obtained for different values of λ with different initial conditions to arrive at the complete representation of the true Pareto front.

It is also very informative to analyze the β profile for some of the points shown in Figure 6. Specifically, in Figure 7, we plot the optimum orientation profile for points corresponding to $\lambda = 0$, $\lambda = 0.2$, and $\lambda = 1000$. We notice that for $\lambda = 0$, the optimum profile involves gradual maneuvers of very low magnitude. As λ increases to a value of 0.2, the orientation profile looks similar but the amplitude of the maneuvers has almost doubled. And finally, for large values of λ, the optimum profile requires attitude maneuvers at the maximum allowed slew rate. The transitions are sharp with β values varying sharply over a wide range of angles from -50° to 50°. As mentioned earlier, sharper transitions in orientation produce more power but require more aggressive orbital maneuvers that demand more propellant. Figures 6 and 7 provide a clear illustration of this concept.

In order to visualize the trajectories of the spacecraft in the ECI frame, we plot snapshots of the trajectories of the spacecraft at six different instances over the course of one orbit in Figure 8 for

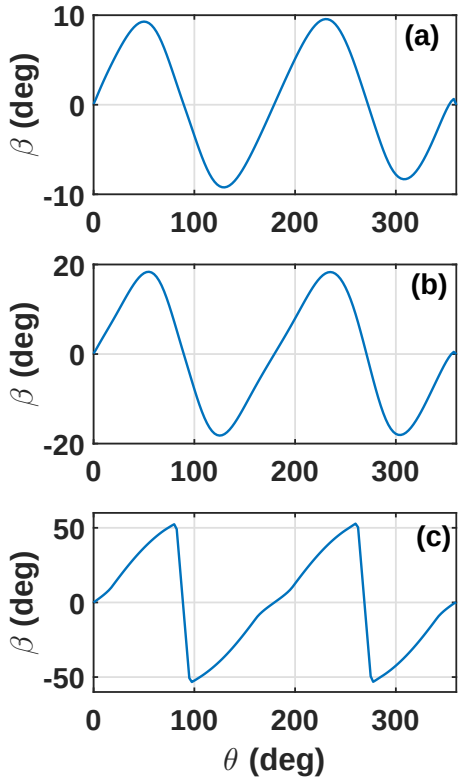

Figure 7. (a), (b) and (c) panels showing the optimum orientation profile for $\lambda = 0$, $\lambda = 0.2$, and $\lambda = 1000$ respectively.

both $\lambda = 0$ and $\lambda = 1000$. These trajectories show how the relative positions of the satellites change over the course of one orbit and have strong similarities with the periodic relative orbits which represent a force-free solution to the linearized equations of relative dynamics in the LVLH frame. While it is very hard to discern the differences in trajectories for different values of λ from these snapshots, the most striking difference appears in the second and fifth frames (compare frame (b) with frame (h) and frame (e) with frame (k)). For large values of λ, this is where there is a sharp transition in the value of β, as shown in Figure 7, corresponding to $\theta = 90^\circ$ and $\theta = 270^\circ$. At these angles, the dual-sided spacecraft transition from using the anti-sun surface to the sun-facing surface and vice versa for RF transmission.

It is worth noting that different satellites in the formation consume different amount of propellant depending on their location and distance from the chief. The propellant mass numbers shown in Figure 6 correspond to the satellite located at the corner of the formation which requires the maximum amount of propellant. For $\lambda = 1000$, the propellant masses needed for different satellites in the formation are shown in Figure 9. It shows that even for satellites at the same initial distance from the chief, the propellant consumption can be significantly different, depending on its relative position in the formation.

In order to better understand the source of this discrepancy, we plot the x, y and z coordinates of four of the 16 satellites in the LVLH frame for $\lambda = 1000$. These plots, shown in Figure 10, correspond to the four blue colored satellites in Figure 9. The blue and purple curves correspond to

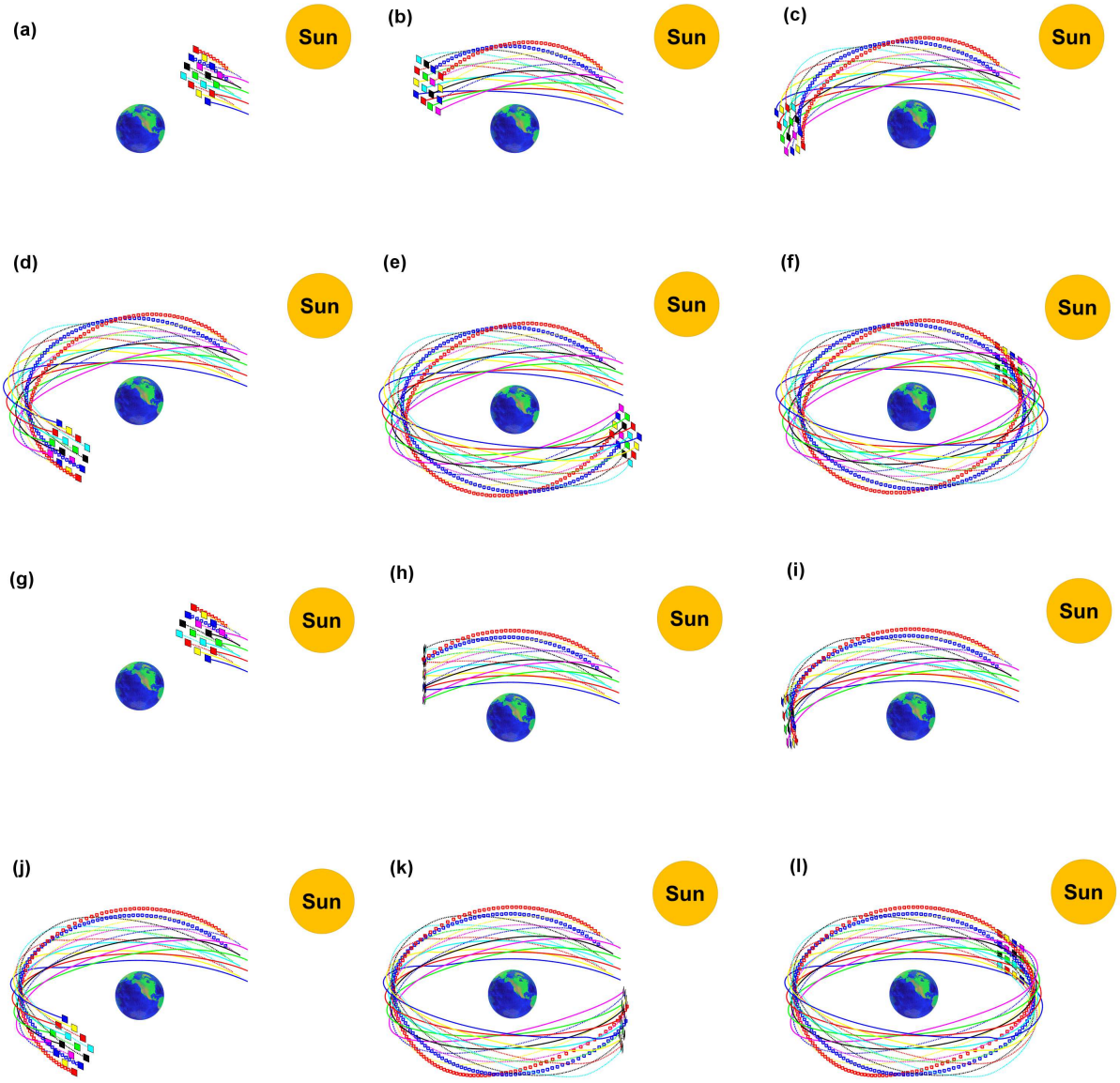

Figure 8. Orbits of deputies in a 4 $\times$ 4 formation. Panels (a) through (f) show the trajectories for $\lambda = 0$ and panels (g) through (l) show the trajectories for $\lambda = 1000$. These plots are from the point of view of an inertial observer over 24 hours. Note that the sizes of objects in this figure are not representative of their actual sizes.

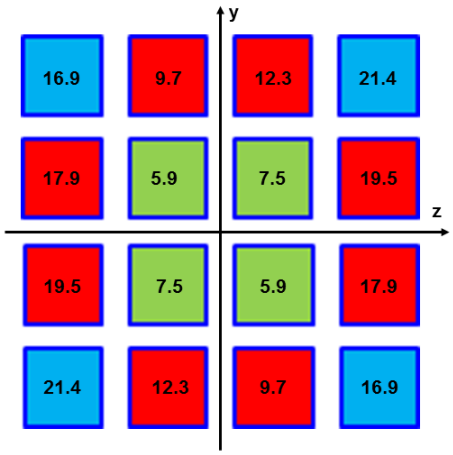

Figure 9. Propellant mass consumption in kg for satellites at different initial positions in the formations. These numbers are obtained by solving the optimization problem for $\lambda = 1000$. Satellites at the same initial distance from the chief are shown in the same color.

the satellite with propellant mass consumption of 21.4 kg while the yellow and orange curves are for satellites with propllant mass of 16.9 kg. Points correspondins to $\theta = 90^\circ$ and $\theta = 270^\circ$ are marked with a black line indicating the locations at which the sharp transition maneuvers shown in Figure 7(c) take place. Due to the planarity constraint, the propellant requirement is dominated by the distance of the satellites from the chief in the $x - y$ plane at these locations. Clearly, the blue and purple satellites are at a larger distance and hence consume more propellant. This can also be seen in Figure 11 which shows the optimum thrust profile for these spacecraft.

CONCLUSIONS AND FUTURE WORK

In this paper, we have outlined the trajectory design problem for space-based solar power using a formation of planar satellites. We discussed how the physics of the problem couples the attitude and orbital dynamics and also showed how the SCP framework can be used to solve the ensuing non-convex optimization problem. Our initial results show that the methodology adopted is capable of producing the desired results. It has allowed us to arrive at useful estimates for the propellant mass needed for a 11-year mission and more importantly, the trade-off analysis helps us pick a design point based on the relative importance of power and mass.

There are numerous ways in which this analysis can be extended in the future. The first obvious direction is to increase the size of the formation to check if the trends observed continue to be valid. We have so far treated the motion of the chief as a known quantity. From the analysis presented by Goel *et al.* (2017),[7] we know that solar radiation pressure has a tendency to ellipticize the orbit. This might increase the amount of propellant needed for maintaining the shape of the formation. It would hence be meaningful to also optimize the chief's orbit, taking into account the influence of solar radiation pressure.

In our analysis, we have also ignored the gravitational influence of the moon and the sun. Typically, geostationary satellites have to carry extra propellant for North-South and East-West station-keeping and will be taken into account in our future analysis efforts. While all the results in this paper are for a geosynchronous formation, the analysis can also be extended to a LEO formation

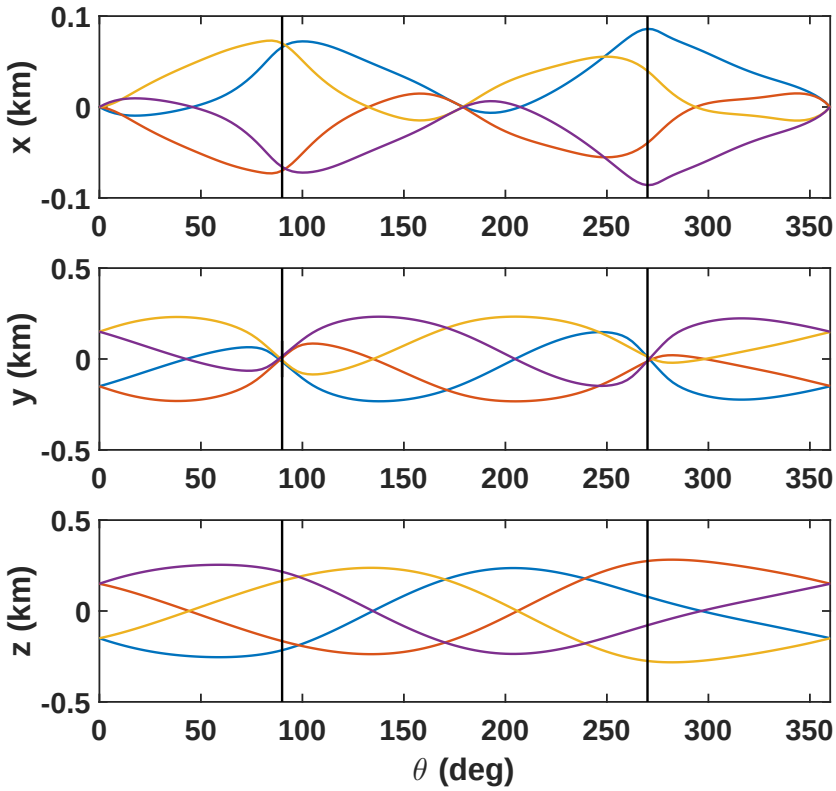

Figure 10. x, y **and** z **coordinates of the four corner spacecraft from Figure 9 for** $\lambda = 1000$**.** $\theta = 90^\circ$ **and** $\theta = 270^\circ$ **locations are marked with a black line corresponding to the points with sharp maneuvers and hence maximum control input requirement.**

where the challenges are quite different since we cannot target a single receiving station on the Earth. We also have to contend with significant amount of eclipse time in each orbit, in addition to the J2 and drag perturbation forces.

The sequential convex programming approach is not guaranteed to find the global optimum and it would be useful in the case of this specific problem to obtain some theoretical bounds or identify the conditions under which convergence and more importantly, convergence to a global minimum can be proved. It would also be useful to compare the results obtained from this approach with those obtained using ideas of relative orbital motion with the HCW equations. It would also be desirable to estimate the computational efficiency of the algorithm, especially for large formations and study how it gets affected by changes to the trust region update scheme. Finally, it would be useful to check the accuracy of these solutions against other algorithms such as genetic algorithms and simulated annealing.

In the future, the planarity and array maintenance constraints can also be gotten rid of by developing a cost function that can estimate the performance of the system for non-planar formations with gaps among the modules, taking into account the PV and RF shadowing effects.

As mentioned in the Problem Formulation section, trajectory design is only one of the numerous guidance and control problems associated with space-based solar power. The reconfiguration

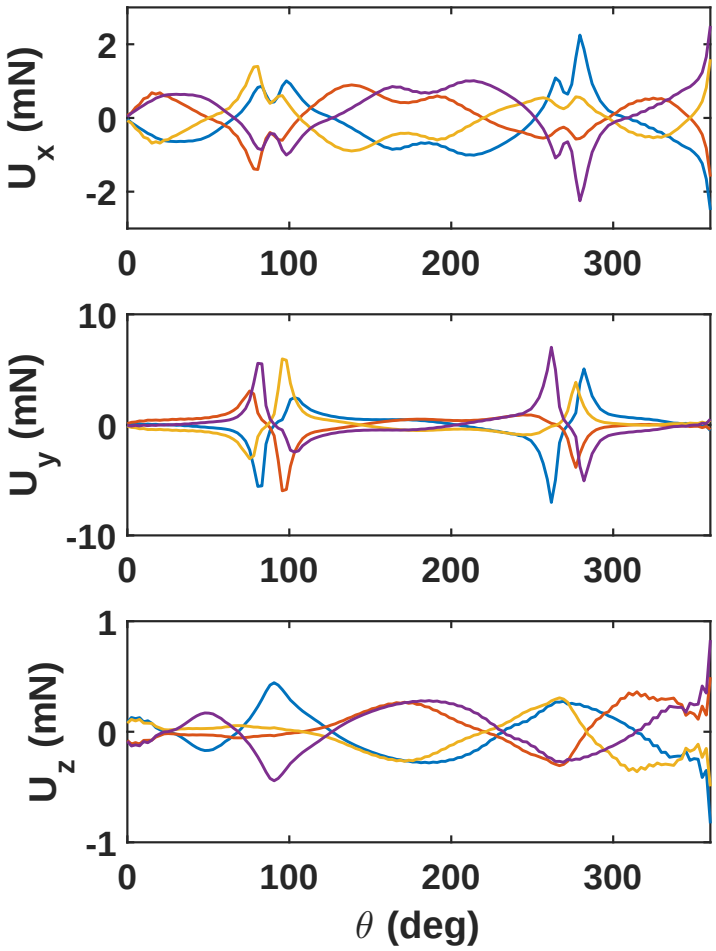

Figure 11. The optimum thrust profile in the x, y and z directions for the four corner spacecraft from Figure 9 for $\lambda = 1000$.

problem seems to be directly linked with the trajectory design problem since it might influence the total propellant mass needed for the mission. The methodology presented in this paper could also be extended for solving these related problems.

ACKNOWLEDGMENTS

The authors thank Northrop Grumman Corporation for supporting this project. We also thank all other members of the SSPI team at Caltech for their valuable inputs.

APPENDIX A: EQUATIONS FOR LINEARIZED DYNAMICS

$A_j(k)$, $B_j(k)$ and $c_j(k)$ are given by the following expressions

$$A_j(k) = e^{A(\bar{\mathbf{x}}_j(k))\Delta t} \tag{10}$$

$$B_j(k) = \int_0^{\Delta t} e^{A(\bar{\mathbf{x}}_j(k))\tau} B d\tau \tag{11}$$

$$c_j(k) = \int_0^{\Delta t} e^{A(\bar{\mathbf{x}}_j(k))\tau} c(\bar{\mathbf{x}}_j(k)) d\tau \tag{12}$$

$A(\mathbf{x_j}(\mathbf{k}))$ is given by

$$A(\mathbf{x_j}(\mathbf{k})) = \begin{bmatrix} 0_{3\times 3} & I_3 \\ G_{3\times 3} & \begin{matrix} 0 & 2\omega_z & -2\omega_y \\ -2\omega_z & 0 & 2\omega_x \\ 2\omega_y & -2\omega_x & 0 \end{matrix} \end{bmatrix}$$

where $\vec{\omega} = [\omega_x, \omega_y, \omega_z]$ is the rotational angular velocity vector of the chief, $0_{3\times 3}$ is the 3×3 null matrix and I_3 is the 3×3 identity matrix. $G_{3\times 3}$ is given by

$$G_{3\times 3} = \begin{bmatrix} \dot{\theta}^2 - \frac{\mu}{r_j^5}\frac{3\mu z(x+r)}{r_j^5} + \frac{3\mu r x}{r_j^5} & \ddot{\theta} + \frac{3\mu y(x+r)}{r_j^5} & \frac{3\mu z(x+r)}{r_j^5} \\ -\ddot{\theta} + \frac{3\mu y x}{r_j^5} & \dot{\theta}^2 - \frac{\mu}{r_j^5}(r_j^2 - 3y^2) + \frac{3\mu r x}{r_j^5} & \frac{3\mu z y}{r_j^5} \\ \frac{3\mu z x}{r_j^5} & \frac{3\mu z y}{r_j^5} & -\frac{\mu}{r_j^5}(r_j^2 - 3z^2) \end{bmatrix}$$

B is just a selection matrix given by

$$B = \begin{bmatrix} 0_{3\times 3} \\ I_3 \end{bmatrix}$$

$c(\mathbf{x_j}(\mathbf{k}))$ is given by

$$c(\mathbf{x_j}(\mathbf{k})) = \begin{bmatrix} 0 \\ 0 \\ 0 \\ -\frac{3\mu(x+r)}{r_j^3} + \mu r\left(\frac{1}{r^3} - \frac{1}{r_j^3}\right) \\ \frac{3\mu y}{r_j^3} \\ \frac{3\mu z}{r_j^3} \end{bmatrix}$$

REFERENCES

[1] I. Asimov, "Reason," *I, Robot*, 1941, pp. 59–77.

[2] P. E. Glaser, "Power from the sun: its future," *Science*, Vol. 162, No. 3856, 1968, pp. 857–861.

[3] J. C. Mankins, "SPS-ALPHA: The first practical solar power satellite via arbitrarily large phased array (a 2011-2012 NASA NIAC phase 1 project)," *Artemis Innovation Management Solutions LLC*, 2012.

[4] J. C. Mankins, "A technical overview of the Suntower solar power satellite concept," *Acta Astronautica*, Vol. 50, No. 6, 2002, pp. 369–377.

[5] S. Sasaki, K. Tanaka, K. Higuchi, N. Okuizumi, S. Kawasaki, N. Shinohara, K. Senda, and K. Ishimura, "A new concept of solar power satellite: Tethered-SPS," *Acta Astronautica*, Vol. 60, No. 3, 2007, pp. 153–165.

[6] M. Arya, N. Lee, and S. Pellegrino, *Ultralight Structures for Space Solar Power Satellites*. AIAA SciTech, American Institute of Aeronautics and Astronautics, 2016, doi:10.2514/6.2016-195010.2514/6.2016-1950.

[7] A. Goel, N. Lee, and S. Pellegrino, "Trajectory Design of Formation Flying Constellation for Space-Based Solar Power," *Aerospace Conference, 2017 IEEE*, IEEE, 2017.

[8] J. A. Atchison and M. A. Peck, "Length scaling in spacecraft dynamics," *Journal of guidance, control, and dynamics*, Vol. 34, No. 1, 2011, pp. 231–246.

[9] D. P. Hamilton and A. V. Krivov, "Circumplanetary dust dynamics: Effects of solar gravity, radiation pressure, planetary oblateness, and electromagnetism," *Icarus*, Vol. 123, No. 2, 1996, pp. 503–523.

[10] I. M. Ross, "6 Space Trajectory Optimization and," *Modern astrodynamics*, Vol. 1, 2006, p. 155.

[11] J. Schulman, J. Ho, A. X. Lee, I. Awwal, H. Bradlow, and P. Abbeel, "Finding Locally Optimal, Collision-Free Trajectories with Sequential Convex Optimization," *Robotics: science and systems*, Vol. 9, Citeseer, 2013, pp. 1–10.

[12] F. Augugliaro, A. P. Schoellig, and R. D'Andrea, "Generation of collision-free trajectories for a quadrocopter fleet: A sequential convex programming approach," *Intelligent Robots and Systems (IROS), 2012 IEEE/RSJ International Conference on*, IEEE, 2012, pp. 1917–1922.

[13] D. Morgan, S.-J. Chung, and F. Y. Hadaegh, "Model predictive control of swarms of spacecraft using sequential convex programming," *Journal of Guidance, Control, and Dynamics*, Vol. 37, No. 6, 2014, pp. 1725–1740.

[14] D. Morgan, S.-J. Chung, and F. Hadaegh, "Spacecraft swarm guidance using a sequence of decentralized convex optimizations," *AIAA/AAS Astrodynamics Specialist Conference*, 2012, p. 4583.

[15] D. Morgan, G. P. Subramanian, S.-J. Chung, and F. Y. Hadaegh, "Swarm assignment and trajectory optimization using variable-swarm, distributed auction assignment and sequential convex programming," *The International Journal of Robotics Research*, Vol. 35, No. 10, 2016, pp. 1261–1285, doi:10.1177/0278364916632065.

[16] S.-J. Chung and R. Foust, "Solving Optimal Control with Nonlinear Dynamics Using Sequential Convex Programming," in prep.

[17] M. Grant, S. Boyd, and Y. Ye, "CVX: Matlab software for disciplined convex programming," 2008.

[18] E. Anderson and K. Anderson, "MOSEK: High performance software for large-scale LP, QP, SOCP, SDP and MIP including interfaces to C, Java, MATLAB, .NET and Python," *MOSEK, Copenhagen*, 2012.

[19] D. Bock, M. Bethge, and M. Tajmar, "Highly Miniaturized FEEP Thrusters for CubeSat Applications," *Proceedings of the 4th Spacecraft Propulsion Conference, Cologne*, Vol. 2967498, 2014.

[20] R. S. Legge and P. C. Lozano, "Electrospray propulsion based on emitters microfabricated in porous metals," *Journal of Propulsion and Power*, Vol. 27, No. 2, 2011, pp. 485–495.

[21] J. P. Sheehan, T. A. Collard, F. H. Ebersohn, and B. W. Longmier, "Initial Operation of the CubeSat Ambipolar Thruster," *34th International Electric Propulsion Conference*, 2015.

[22] P. Sheehan, T. Collard, B. W. Longmier, and I. Goglio, "New low-power plasma thruster for nanosatellites," *Propulsion and Energy Forum. American Institute of Aeronautics and Astronautics*, 2014.